Scripta Materialia 212 (2022) 114550

Contents lists available at ScienceDirect

Scripta Materialia

journal homepage: www.elsevier.com/locate/scriptamat

Linking through-thickness cracks in metallic thin films to in-situ electrical resistance peak broadening

David D. Gebhart[a,*], Anna Krapf[b], Christoph Gammer[a], Benoit Merle[b], Megan J. Cordill[a]

[a] Erich Schmid Institute of Materials Science, Austrian Academy of Sciences, Jahnstrasse 12, Leoben 8700, Austria
[b] Department of Materials Science & Engineering, Institute 1, University of Erlangen-Nürnberg (FAU), Martensstrasse 5, Erlangen 91058, Germany

ARTICLE INFO

Article history:
Received 10 December 2021
Revised 18 January 2022
Accepted 19 January 2022

Keywords:
Nanocrystalline metal
Thin films
Fatigue
Electrical resistivity
Through-thickness cracks

ABSTRACT

Measurements of electrical resistance have been used extensively as a failure criterion in cyclically loaded conductive films. However, not much research has been performed on extracting additional information contained within such resistance data sets. This study shows that an increase in peak width evidences a transition from cracks bridging to through-thickness crack formation. A Au/Cr bilayer system on a polyimide substrate is used for data generation but the method is applicable to any material system where both necking and through-thickness cracks are formed and no immediate formation of electrically insulating oxide layers occurs upon damage initiation. The method is easy to implement, and has the ability to replace time-intensive and destructive inspection methods.

© 2022 The Authors. Published by Elsevier Ltd on behalf of Acta Materialia Inc.
This is an open access article under the CC BY license (http://creativecommons.org/licenses/by/4.0/)

Electrically conductive metal coatings are an integral part in a wide variety of applications. Carrying either signals or power, they are present in an abundance of electronic devices and applications, such as sensors, microelectromechanical systems (MEMS), display technology applications, and photovoltaic cells. Many of those applications involve bending and stretching, where mechanical or thermomechanical strain is introduced into the system. As the failure of a single electrical connection can lead to failure of the whole device, we need to understand their cyclic behaviour and fracture mechanisms in order to create long lasting devices. A well established method to investigate such failures is performing in-situ electrical resistance measurements while cyclic tensile or bending loads are applied to the system. Such investigations have been carried out for a wide variety of systems, such as Ag [1–3], Cu [4–6], Al [5], Au [7], Au/Ti [8], and Mo/W [9] on polymer substrates.

Most studies are concerned with the optimization of fatigue lifetimes of different material systems and use an increase in electrical resistance only as a failure criterion [1–9] and very little analysis has been performed to extract further information contained within resistance data. Gence et al. [10] used resistance curve amplitude and curve minima evolution, as well as curve shape continuity, in bending tests to argue robustness of TiN-Ag nanowire nanocomposite coatings. Other studies have discovered a double resistance peak in conductive coatings [11,12] which has been found by Graz et al. [12] to be caused by lateral contraction and closure of cracks that have formed parallel to the load direction.

While some system parameters, such as mean grain size, will have a small influence on the electrical resistivity of a conducting material [13], larger changes in conducting film electrical resistance are mostly a function of crack length and crack density in the film. An empirical model was found from finite element simulations, giving the relation of electrical resistance and the (square) product of crack density and crack length (with cracks perpendicular to straining direction) [14]:

$$\frac{R}{R_0} = 1 + \frac{C_l l_0}{\sqrt{2}} + \frac{C_l^2 l_0^2}{2} \quad (1)$$

with resistance R, initial resistance R_0, linear crack density C_l, and average crack length l_0. Crack length and crack density cannot be separated within single direct current resistance data points. However, thorough analysis of ensembles of electrical resistance data points could bring more insights.

This work analyzes full width at half maximum (FWHM) values of resistance peaks measured during cyclic uniaxial loading. Fig. 1 gives an overview of the analyzed data for one randomly chosen measurement series. All collected data points are shown in Fig. 1(a), an enlarged region of 10 cycles is given in (b), and (c) presents only one cycle. Here, the FWHM is measured from the linear interpolated data at approximately 0.5 cycle durations. A material system of 160 nm Au on polyimide, with a 50 nm Cr

* Corresponding author.
E-mail address: david.gebhart@oeaw.ac.at (D.D. Gebhart).

https://doi.org/10.1016/j.scriptamat.2022.114550
1359-6462/© 2022 The Authors. Published by Elsevier Ltd on behalf of Acta Materialia Inc. This is an open access article under the CC BY license (http://creativecommons.org/licenses/by/4.0/)

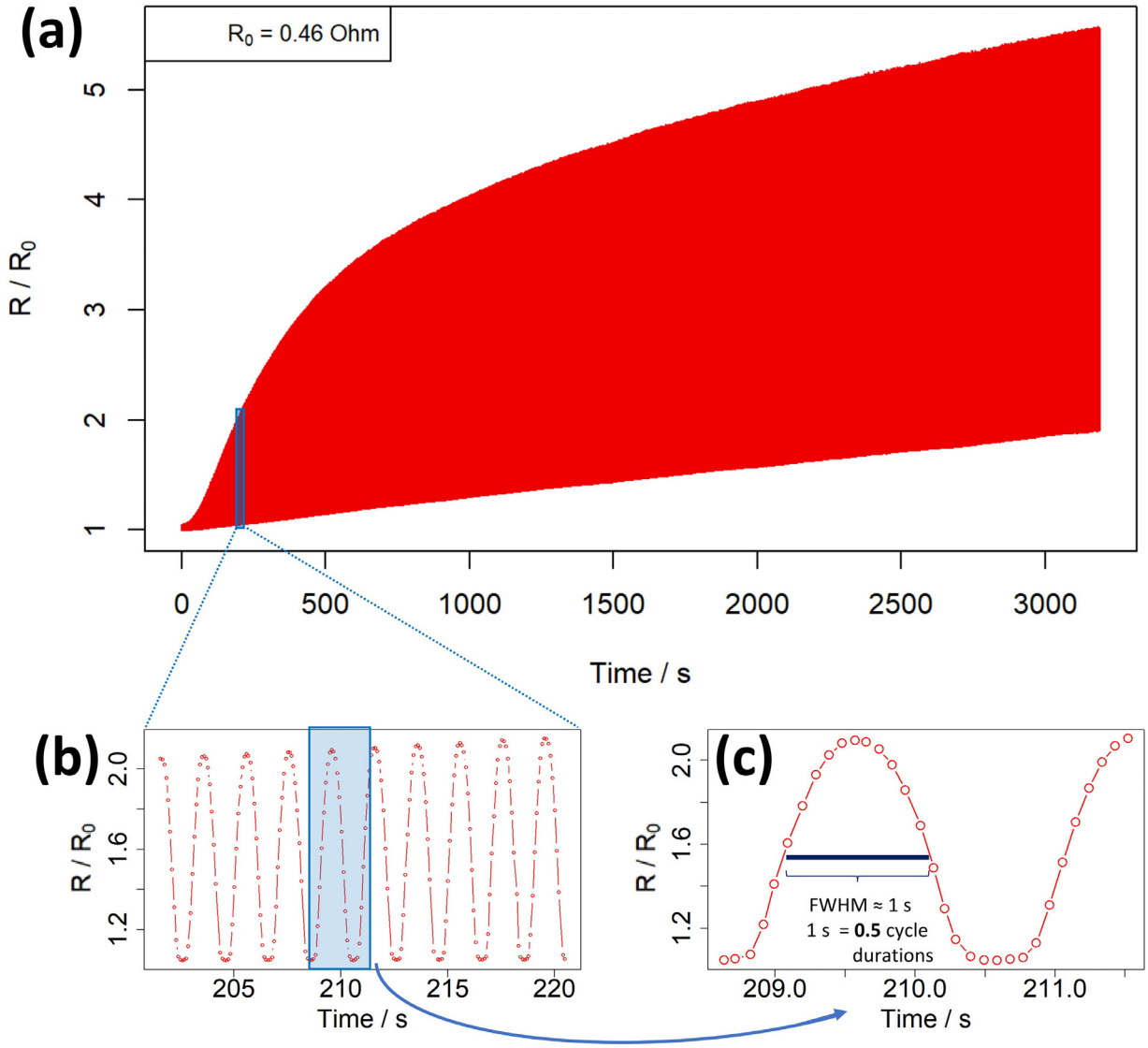

Fig. 1. One measurement series - overview of acquired data: (a) All collected data points, (b) an enlarged region of 10 cycles, and (c) only one cycle with a FWHM value of approximately 0.5 cycle durations.

interlayer, was used. Au is a face centered cubic (fcc) metal that shows rather ductile fracture properties, while the body centered cubic (bcc) metal Cr behaves more brittle and has a lower fracture strain than Au [15]. In such a system, cracks first form in the brittle interlayer, they serve as stress concentration points, and induce damage in the ductile layer [15–17]. The system is of scientific interest because Au shows good properties and robustness as an electrical conductor and the Cr interlayer critically improves adhesion to the polymer substrate. It has been shown that monotonic straining of similar material systems first leads to localized necking in the ductile fcc metal film at interlayer-induced stress concentration points, before through-thickness cracks (TTCs) form Cordill and Marx [18], Kreiml et al. [19]. Differentiating between TTCs and necking is widely acknowledged as challenging, even with the usual microscopy methods [20].

The Cr and Au films were deposited onto a 50 × 50 mm^2 polyimide substrate of a thickness of 50 µm (Upilex-S; Ube Industries, Ltd.) with a custom-built thermal evaporation unit at a chamber pressure between 10^{-7} and 10^{-6} mbar. First, a 50 nm Cr layer was deposited at a rate of 0.4–0.5 Å/s and a substrate temperature of 150 °C. On top of this layer, a 160 nm Au layer was deposited at a rate of around 1 Å/s and a substrate temperature of 80 °C. Deposition rates and thicknesses were measured with a quartz crystal oscillator and the substrate temperature was measured with a thermocouple positioned close to the substrate. The sample was rotated at 10 rpm during evaporation. The mean grain diameter of the deposited gold film was determined to be 129 nm with electron backscatter diffraction measurements and (111) texture was observed. After deposition, the sheet was cut into 6 × 25 mm^2 rectangles, using a Cricut Explore Air 2 (Cricut, Inc.). The samples were cyclically loaded under strain control using a Tytron 250 Microforce Testing System (MTS Systems). A sinusoidal load was applied at a frequency of 0.5 Hz, 2% peak strain, and non-zero minima strain of 0.2% to prevent sample buckling due to non-negligible plastic deformation of the polyimide substrate. The samples were fastened with a custom-built clamp made of a dielectric bottom and a metallic top section with two attached pins on each side, similar to Glushko and Cordill [21], leaving a 6 × 15 mm^2 gauge section to be strained. The set-up was connected to a Keithley 2000 Multimeter for four-wire resistance measurements. The multimeter's power line cycle (PLC) was set to 1, with a 50 Hz line frequency, to suppress noise in the data. Automated data acquisition was performed using a Sparkfun GPIB-USB Controller (BOB-00549) and controlled by a Scilab script, achieving a sampling rate

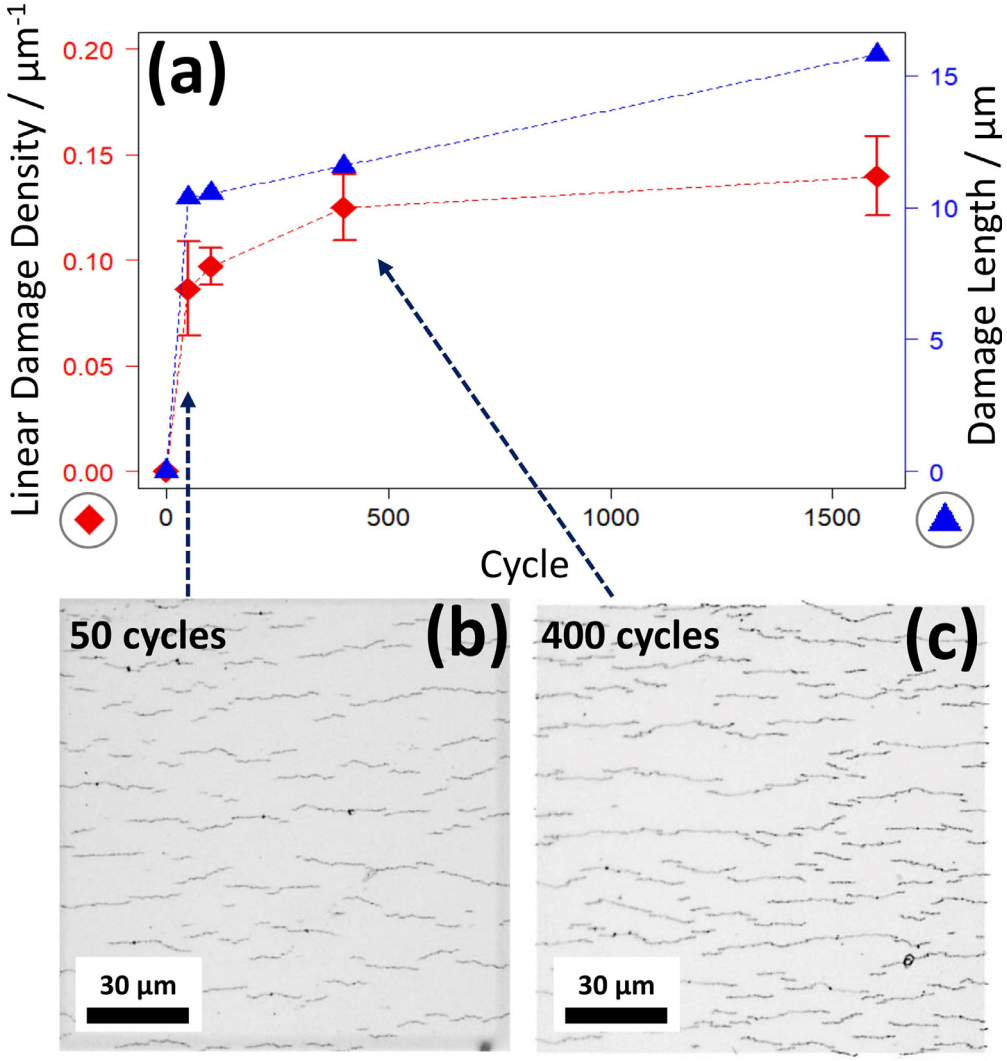

Fig. 2. (a) Linear damage density (red diamonds) and average damage length (blue triangles; note: no clear unimodal distribution - no width of distribution given in plot). Micrographs after (b) 50 and (c) 400 applied strain cycles. (For interpretation of the references to colour in this figure legend, the reader is referred to the web version of this article.)

of around 10 samples s^{-1}. The microstructural characterization was performed by scanning electron microscopy (SEM, Zeiss LEO 1525) imaging of samples loaded to 2% strain with a custom-built mechanical device with clamps similar to those used in cyclic straining. Focused ion beam (FIB) cross-sections were prepared with a Zeiss LEO 1540XB. To measure linear damage density and damage length, light microscopy images were used. It should be noted that damage has the appearance of cracks in micrographs but since not all apparent cracks penetrate the whole thickness of the film, they will be referred to as damage. For linear damage densities, the number of damage sites intersecting lines parallel to straining direction (at least 700 µm combined) was divided by the total length of all drawn lines. For damage length measurements, an area of 20 × 100 μm^2 (the smaller length being perpendicular to the loading direction) was taken and for all damage sites touching this area, their spread perpendicular to the straining direction was measured - the number of damage sites measured was $\geq$ 28 for all samples. The data was analyzed by a script written in the programming language *R*. For calculation of resistance FWHM values, the function *approxfun* was used to create linear interpolations between measured points. The *x*-distance between rising and falling interpolations was taken at their intersections with the value bisecting the previous minimum and the current peak maximum.

Fig. 2 (a) depicts linear damage density (red diamonds) and average damage length (blue triangles) up to 1600 cycles. The data sets (length and density) were constructed from different samples from the same deposition run. They were tested to a different number of cycles to avoid interrupting cycling to perform damage analysis. Most damage visible in the micrographs (shown in Fig. 2(b) and (c)) occurs at very low cycle numbers, below 50. For both damage density and damage length, the increase between cycles 50–100 is approximately an order of magnitude smaller than the initial increase up to cycle 50.

Fig. 3 (a) shows the maximal resistance for each individual cycle up to cycle 1600, given as a mean with one sample standard deviation, taken from four measurement series and normalized to each sample's initial resistance R_0. The increase in average resistance (local slope of the solid black curve) is reaching a maximum after cycle 50, while the damage density and length have already started to level off at that point (compare Fig. 2(a) with Fig. 3(a)). Resistance maxima even continue to increase linearly up to around cycle 300 (see Fig. 3(a)). The delayed increase of the resistance compared to the crack density and length could be an indication that the early damage visible in micrographs does not immediately extend through the whole film thickness and TTCs only develop with further cycling. For TTCs, Eq. (1) predicts larger resis-

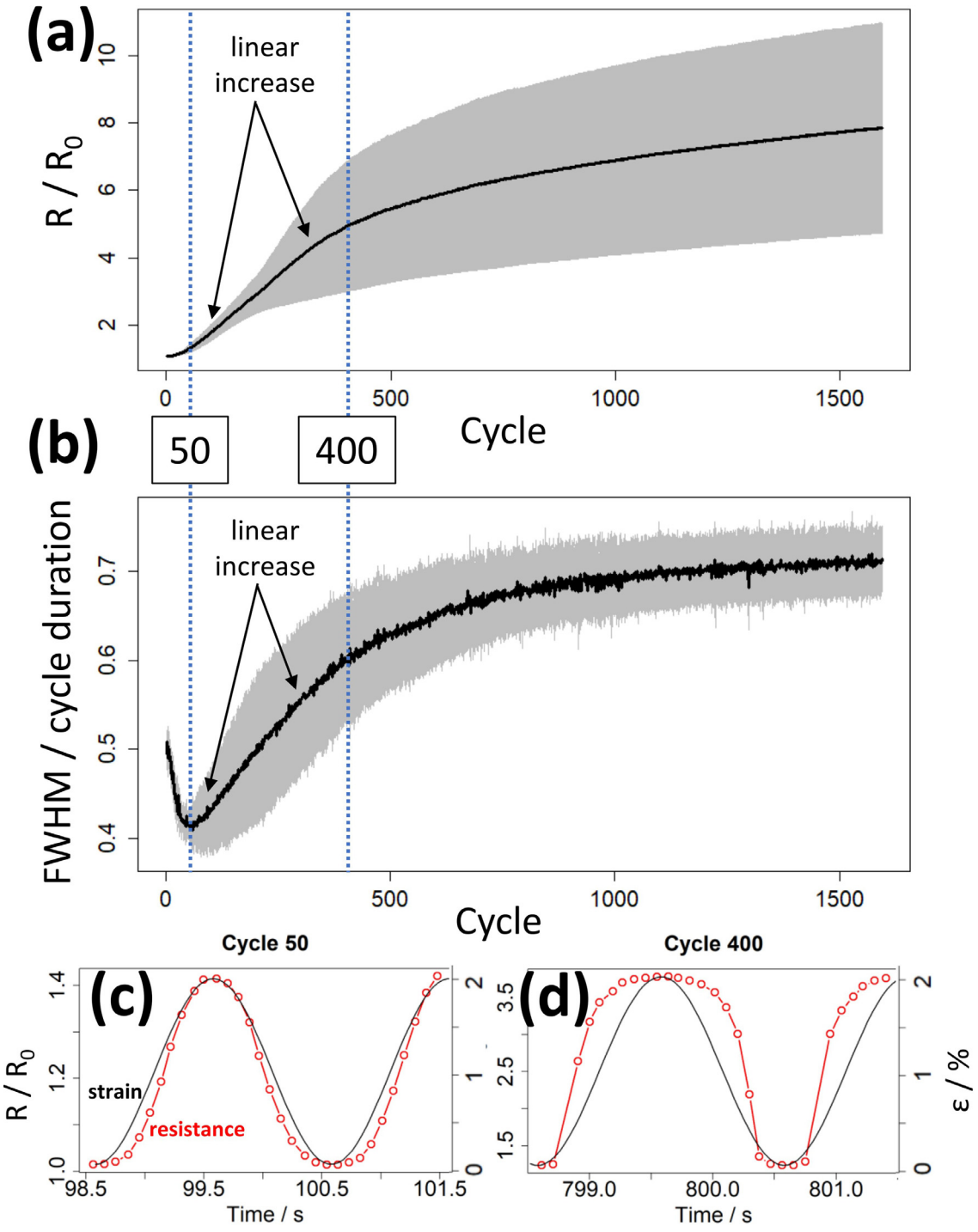

Fig. 3. (a) Maxima resistance data points for each cycle normalized to initial resistance - mean ± 1 sample standard deviation (s) (4 measurement series). (b) Full width at half maximum for each cycle - mean ± 1 s (4 measurement series). Resistance peaks of one measurement series of cycles (c) 50 and (d) 400 in red with the sinusoidal strain curve overlayed in black. (For interpretation of the references to colour in this figure legend, the reader is referred to the web version of this article.)

tance values than measured for early cycles and smaller values for later cycles. At cycle 50 it would yield a value of 2.2 R_0, larger than the measured peak value of 1.3 R_0, and only at cycle 400 would it drop below the measured value of 4.9 R_0, with a model value of 3.1 R_0. Note that the model assumes all cracks to be of the exact same length and might underestimate the electrical resistance compared to a realistic, wider distribution. However, the model still shows an earlier increase in resistance than the measurements. This is a clear indication that a process of damage propagation is happening which cannot be captured by surface micrographs. One such process would be the evolution of surface cracks (necking) to TTCs.

The data also features a distinct and highly repeatable broadening of resistance peaks with increasing cycle numbers. This is shown in the plot of full width at half maximum (FWHM) values in Fig. 3(b), with a value of 1 representing a full cycle duration. The data depicted comes from the same four measurement series shown in Fig. 3(a). As a reference, note that a perfect sinusoidal curve would show a FWHM value of 0.5 cycle durations. As can be seen in Fig. 3(c) and (d), early resistance peaks are narrower than

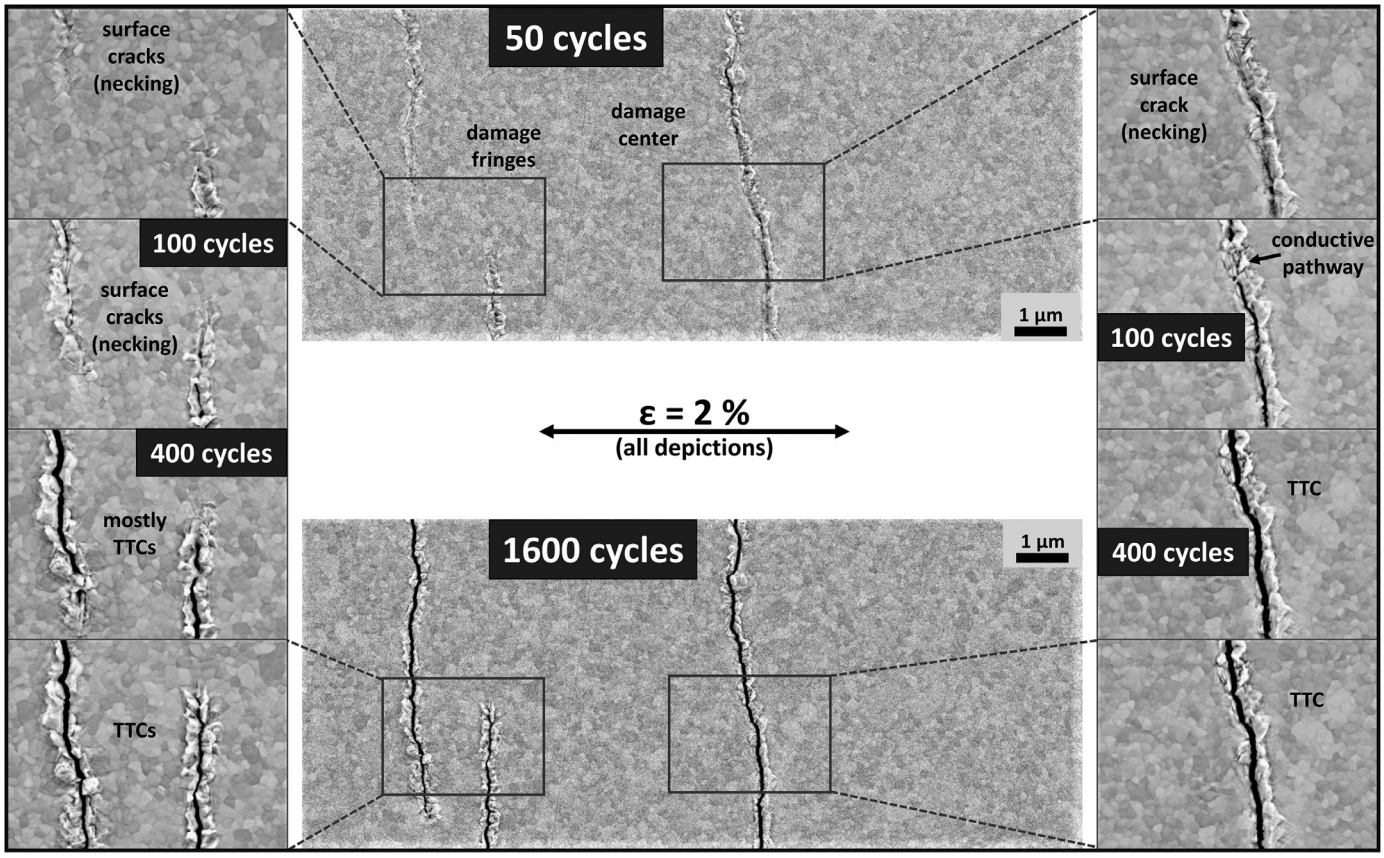

Fig. 4. SEM images of the same sample region at 2% strain (loaded) after 50, 100, 400, and 1600 applied strain cycles (top to bottom).

the strain peaks while later peaks are broader. The strain signal remains sinusoidal in either case, exhibiting a constant FWHM value of 0.5.

The initial drop in electrical FWHM values can be correlated to the extensive damage formation and propagation visible in the micrographs up to cycle 50 (see Fig. 2). The decrease in FWHM is an indication that this damage is formed around strain maxima, because this leads to a spike in resistance centered around strain maxima, thus making the peaks more pointed and narrow. Please note that it was confirmed by SEM micrographs taken after 5 and 10 cycles (not shown here) that most damage in the Au layer does not form immediately during the very first cycles but rather there is continuous damage formation and propagation at early cycle numbers.

After the initial decrease, the FWHM plot shows similar trends as the peak resistance values in Fig. 3(a). Both show a maximum and almost constant slope between cycles 50 and 300 and both start to level off with further cycling. The FWHM values are simply a measurement of how quickly electrical resistance rises within one cycle. With sinusoidal strain, a FWHM value greater than 0.5 means that the electrical resistance increases faster than the applied strain. The resistance peak of cycle 400 in Fig. 3(d) shows a very steep increase at low strain values which then almost transitions to a plateau around the strain maximum. Cracks which have not propagated through the whole film thickness will include metallic bridging ligaments electrically connecting the crack faces. The electrical resistance of a sample is relative to the mean conductive cross-section between crack faces and a plateau in a resistance peak signifies that cracks are completely opened and that their conductive cross-sections are not further decreased with increasing strain (cracks/damage do not propagate further either through the film or laterally in-plane). The more electrically conductive bridges between crack faces break during cycling, the more pronounced this plateau will become and the higher the FWHM value will be. With a reduction in conductive cross-section between crack faces, TTCs are forming and propagating which leads to a more complete crack opening at smaller strain values and increases the FWHM values. This means that a rise in FWHM values is a good indication of the formation of TTCs which can otherwise only be detected with extensive inspection methods, such as Focused Ion Beam (FIB) cross-sectioning.

To affirm the relation between FWHM and through-thickness cracking, SEM images of samples loaded to 2% strain are depicted in Fig. 4. SEM images of FIB cross-sections of unloaded damage sites are presented in Fig. 5. It is confirmed that necking does occur, as it was observed in literature [15–19]. With damage growing both from the surface and the substrate, it can be assumed that the black center lines observed at higher cycle numbers in Fig. 4 are TTCs. After 50 cycles, no clear TTCs can be made out and large parts of the damage sites are surface cracks. Only after 100 cycles, some damage has evolved into TTCs. However, there still seem to be bridges at damage centers which are not opened at 2% strain, leading to conductive pathways between crack faces (see inset on right side of Fig. 4) and damage fringes are mostly surface cracks (inset on left side of Fig. 4). Generally, many damage sites form during the first 100 cycles and significant proportions are not yet full TTCs at maximum strain. This is in line with a FWHM value of below 0.5 cycle durations at that range, which indicates pronounced damage propagation around strain maxima along with conductive pathways across damage sites at maximum strain. From cycle 100 to cycle 400, FWHM shows its maximum increase and rises from around 0.45 to 0.6 cycle durations, indicat-

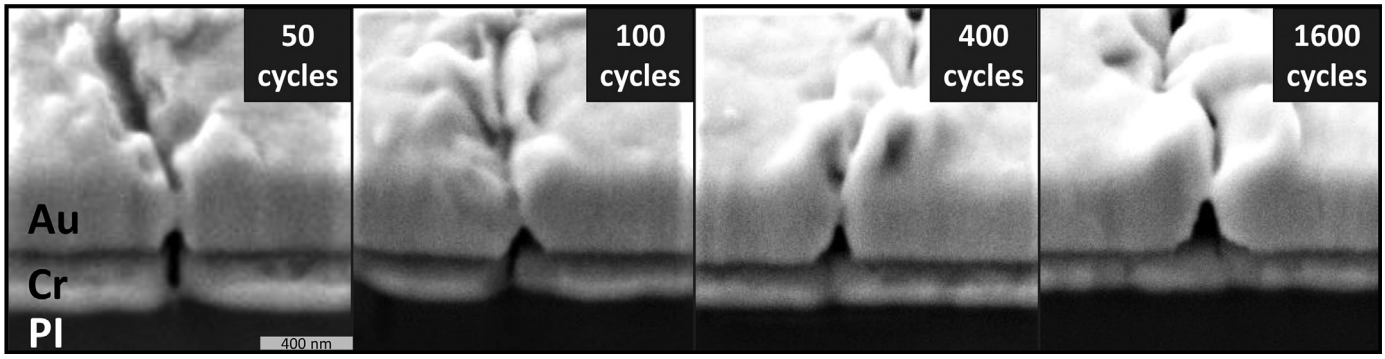

Fig. 5. SEM images of FIB cross-sections at damage sites after 50, 100, 400, and 1600 applied strain cycles (unloaded). Imaged at a 36° angle (0° being in-plane) - scale bar only valid in *x*-dimension. Note: different damage sites imaged.

ing further development of TTCs. This is also where most TTC formation is observed in SEM images. After 400 cycles, damage center regions show a pronounced black center line and even damage fringes have in large part become TTCs. With further loading to 1600 cycles, only slight changes can be observed - damage fringes have developed into TTCs up to the very tip of the damage sites, fitting a slower FWHM increase from 0.6 to 0.7 cycle durations and an onset of saturation (see Fig. 3(b)). Here, the damage sites (now TTCs) are fully opened at the strain maximum and hardly any conductive pathways form when strain is slightly reduced, leading to almost constant electrical resistance around the strain maximum and steep resistance slopes at strain values where cracks open/close. This results in broad resistance peaks and a FWHM value well above 0.5 cycle durations.

To the best of our knowledge, this is the first qualitative report on the importance of FWHM analysis in cyclic loading investigations. This new concept gives access to crack opening characteristics, which could so far not be tracked from using resistance maxima and minima. In addition to general measurements of increase in electrical resistance that describe the total amount of accumulated damage, peak widths can provide more insight into the type of damage present in a sample, either TTC or necking. As a first demonstration, it was shown that FWHM values can be used to detect through-thickness cracks. With FWHM reflecting crack opening and closure properties within a loading cycle, such an analysis has a strong application potential to other investigations. The method is very simple to implement and with enough measurement precision, it could be applied to fatigue experiments in bulk materials, such as crack propagation in notched specimens, as well as more complex fracture mechanics investigations, such as crack closure in fatigue loading.

Funding

This work was supported by the Austrian Science Fund (FWF) [Project I 4384-N] and the German Research Foundation (DFG) [grant ME-4368/8] within the framework of the D-A-CH cooperation FATIFACE.

All data supporting the findings of this study is available from the corresponding author upon reasonable request.

Declaration of Competing Interest

The authors declare that they have no known competing financial interests or personal relationships that could have appeared to influence the work reported in this paper.

References

[1] G.-D. Sim, Y.-S. Lee, S.-B. Lee, J.J. Vlassak, Mater. Sci. Eng. A 575 (2013) 86–93, doi:10.1016/j.msea.2013.03.043.
[2] H. Wan, X. Luo, X. Li, W. Liu, G. Zhang, Mater. Sci. Eng. A 676 (2016) 421–426, doi:10.1016/j.msea.2016.09.010.
[3] Y.-S. Lee, G.-D. Sim, J.-S. Bae, J.-Y. Kim, S.B. Lee, Mater. Lett. 193 (2017) 81–84, doi:10.1016/j.matlet.2017.01.111.
[4] B.-J. Kim, H.-A.-S. Shin, J.-H. Lee, T.-Y. Yang, T. Haas, P. Gruber, I.-S. Choi, O. Kraft, Y.C. Joo, J. Mater. Res. 29 (2014) 2827–2834, doi:10.1557/jmr.2014.339.
[5] X.J. Sun, C.C. Wang, J. Zhang, G. Liu, G.J. Zhang, X.D. Ding, G.P. Zhang, J. Sun, J. Phys. D 41 (2008) 195404, doi:10.1088/0022-3727/41/19/195404.
[6] J. Zhang, X. Zhang, G. Liu, R. Wang, G. Zhang, J. Sun, Mater. Sci. Eng. A 528 (2011) 7774–7780, doi:10.1016/j.msea.2011.06.083.
[7] X. Luo, G. Zhang, Mater. Sci. Eng. A 702 (2017) 81–86, doi:10.1016/j.msea.2017.07.006.
[8] H.-L. Chen, X.-M. Luo, D. Wang, P. Schaaf, G.P. Zhang, J. Mater. Sci. Technol. (2021), doi:10.1016/j.jmst.2021.02.025.
[9] F. Wang, X.-M. Luo, D. Wang, P. Schaaf, G.P. Zhang, MRS Adv. 4 (2019) 2309–2317, doi:10.1557/adv.2019.252.
[10] L. Gence, M. Escalona, C. Castillo, F. Quero, P. Saikia, R. Wheatley, D.E. Diaz-Droguett, M.J. Retamal, U.G. Volkmann, H. Bhuyan, Nanotechnology 30 (2019) 495705, doi:10.1088/1361-6528/ab416c.
[11] C. Chambers, S.P. Lacour, S. Wagner, Z. Suo, Z. Huang, MRS OPL (2003), doi:10.1557/PROC-769-H10.3.
[12] I.M. Graz, D.P.J. Cotton, S.P. Lacour, Appl. Phys. Lett. 94 (2009) 071902, doi:10.1063/1.3076103.
[13] J.-W. Lim, M. Isshiki, J. Appl. Phys. 99 (2006) 094909, doi:10.1063/1.2194247.
[14] O. Glushko, P. Kraker, M.J. Cordill, Appl. Phys. Lett. 110 (2017) 191904, doi:10.1063/1.4982802.
[15] B. Putz, R.L. Schoeppner, O. Glushko, D.F. Bahr, M.J. Cordill, Scr. Mater. 102 (2015) 23–26, doi:10.1016/j.scriptamat.2015.02.005.
[16] M.J. Cordill, T. Jörg, D.M. Többens, C. Mitterer, Scr. Mater. 202 (2021) 113994, doi:10.1016/j.scriptamat.2021.113994.
[17] V.M. Marx, F. Toth, A. Wiesinger, J. Berger, C. Kirchlechner, M.J. Cordill, F.D. Fischer, F.G. Rammerstorfer, G. Dehm, Acta Mater. 89 (2015) 278–289, doi:10.1016/j.actamat.2015.01.047.
[18] M.J. Cordill, V.M. Marx, Philos. Mag. Lett. 93 (2013) 618–624, doi:10.1080/09500839.2013.830792.
[19] P. Kreiml, M. Rausch, V.L. Terziyska, H. Köstenbauer, J. Winkler, C. Mitterer, M.J. Cordill, Thin Solid Films 665 (2018) 131–136, doi:10.1016/j.tsf.2018.07.054.
[20] O. Glushko, B. Putz, M. Cordill, Thin Solid Films 699 (2020) 137906, doi:10.1016/j.tsf.2020.137906.
[21] O. Glushko, M.J. Cordill, Exp. Tech. 40 (2016) 303–310, doi:10.1007/s40799-016-0040-x.